Efficiencies of master, replica, and multilayer gratings for the soft-x-ray–extreme-ultraviolet range: modeling based on the modified integral method and comparisons with measurements

Leonid I. Goray and John F. Seely

The near-normal-incidence efficiencies of a 2400-groove/mm holographic master grating, a replica grating, and a multilayer grating are modeled in the soft-x-ray–extreme-ultraviolet (EUV) regions and are compared with efficiencies that are measured with synchrotron radiation. The efficiencies are calculated by the computer program PCGrate, which is based on a rigorous modified integral method. The theory of our integral method is described both for monolayer and multilayer gratings designated for the soft-x-ray–EUV-wavelength range. The calculations account for the groove profile as determined from atomic force microscopy with a depth scaling in the case of the multilayer grating and an average random microroughness (0.7 nm) for the short wavelengths. The refractive indices of the grating substrate and coatings have been taken from different sources because of the wide range of the wavelengths (4.5–50 nm). The measured peak absolute efficiency of 10.4% in the second diffraction order at a wavelength of 11.4 nm is achieved for the multilayer grating and is in good agreement with a computed value of ~11.5%. Rigorous modeling of the efficiencies of three similar gratings is in good overall agreement with the measured efficiency over a wide wavelength region. Additional calculations have indicated that relatively high normal incidence efficiency (of at least several percent) and large angular dispersion in the higher orders can be achieved in the 4.5–10.5-nm range by application of various multilayer coatings.

OCIS codes: 050.1950, 050.1960, 260.7200, 310.6860, 340.7470.

1. Introduction

The development during the past decade of manufacturing and measurement techniques for diffraction gratings with various groove profiles, as well as the technology of smooth multilayer coatings for the soft-x-ray–extreme-ultraviolet (EUV)-wavelength range, has resulted in gratings with high experimentally proved values of absolute efficiency for normal incidence.[1–3] The other well-developed type of diffraction periodical structures with high near-normal absolute efficiency[4] are so-called Bragg–Fresnel multilayer gratings produced by etching a profile inside a plane multilayer. Also, a careful comparison has been carried out between the efficiencies measured with x-ray source radiation and those rigorously calculated for several differing types of gratings: a blazed ion-etched master grating,[5] its replica that has several coating layers,[6] another replica with a multilayer MoRu–Be coating,[7] and lamellar multilayer gratings made by etching rectangular grooves in a periodic multilayer stack.[8,9] Performed research has shown not only good agreement between theory and experiment but also good numerical modeling prospects for the accurate efficiency prediction for real gratings used in the soft-x-ray–EUV-wavelength range.

A description of diffraction grating properties in a short-wavelength range on the basis of rigorous vector theories has been considered over a long period of time as problematic owing to the weak numerical convergence of the developed programs and high requirements set for memory and speed of computers.[10] In the soft-x-ray–EUV range an accurate account of shading, absorption, and polarization effects and of the other electromagnetic properties of a grating is required along with an account of small values of the wavelength-to-period ratio and hundreds to thousands of propagating orders.[11] Reliable absolute ef-

L. I. Goray is with the International Intellectual Group, Incorporated, Box 335, Penfield, New York 14526. J. F. Seely (john.seely@nrl.navy.mil) is with the Space Science Division, Naval Research Laboratory, Code 7674, Washington, D.C. 20375.

Received 16 May 2001; revised manuscript received 14 September 2001.

ficiency predictions for relief gratings working in these spectral regions have become possible only after development of effective numerical methods: differential,[12,13] integral,[14,15] and modal.[16] However, rigorous approaches to the modeling of the gratings covered with multilayer coatings, the most promising for these regions, have additional significant difficulties.[17] For example, in Ref. 18 is the rigorous calculation, based on the differential method, for the ideal sawtooth profile of a grating only with a limited number of coating layers and only for the case of TE polarization. For Bragg–Fresnel multilayer gratings, several rigorous models were applied successfully to the study of efficiency behavior: the modal theory[9,19,20] for lamellar gratings and the differential theory[8,21] for various ideal groove geometries. Also the integral approach in the Born approximation[22] was applied to different types of gratings and linear multilayer zone plates. Recently, on the basis of the rigorous modified integral method,[23] a capability has been developed to calculate in the soft-x-ray–EUV spectral range the efficiencies of uncoated gratings,[2,5] gratings with several coating layers,[6] and multilayer gratings[3,7] with any given parameters and, most important, with the real groove profile measured by atomic force microscopy (AFM). A considerable improvement in computers and the perfection of programming techniques enable one to carry out such modeling on a desktop personal computer by using standard operating systems.[24]

A comparison of the measured efficiencies and those calculated by our integral method was presented in Ref. 25 for two gratings, a master[5] and a replica.[6] In Ref. 7, when a computing model developed by its authors and a program was used,[24] qualitative agreement between the theory and the measured efficiency of high-efficiency multilayer gratings at near normal incidence was achieved. The purpose of this research, in which special attention is paid to the problems of theory and the modeling of the efficiencies of real gratings, is to improve the calculated data[25] and to achieve good quantitative agreement between the measurements[7] and the model in a wide wavelength range and for multilayer gratings representing the most difficult type of grating for the calculations. To achieve the latter purpose, we used in the calculations based on the modified integral method a scaled AFM groove profile and the most accurate refractive indices of materials covering a wide spectral range and taken from different sources. In the modeling, both the periodic (groove pattern) and the random component of the averaged groove surface topography (microroughness), which strongly affect the light scattered by a grating in the shortest wavelength range, have been taken into account.

2. Basis of the Modified Integral Method

A real groove profile and its depth have very strong influences on the grating efficiency for small wavelength-to-period ratios. This is true for blazed gratings operating in the soft-x-ray and the EUV range,[5–7] for gratings in this range with other groove profiles,[2,26] for shallow gratings designated for other spectral ranges,[27,28] and for echelle gratings.[29,30] To date the integral method[23] is perhaps the only rigorous method that enables one rather easily to investigate the efficiencies of gratings with real groove profiles in any spectral range. The method is due to the nature of the method itself, when the surface of integration of the surface current coincides with the real surface of the grating border. This is especially true for the described realization of the method in which a groove profile is represented not in a distorted form, by Fourier expansion (for smoothing edge effects[10]), but in an accurate form by means of the collocation points coinciding with points of the real groove profile, thus enabling one to take into account rigorously all jumps of the profile function and its first derivative. Besides, only with such an approach is it possible to calculate the efficiencies of gratings with real profiles that have microroughness fine structures that are especially important in the soft-x-ray–EUV range.

In this section the bases of the integral method theory are considered briefly, and the integral equation for an uncoated grating with finite conductivity and with any arbitrary groove profile is obtained for the case of TE polarization. A more detailed derivation of the integral equations for the case of TM polarization, as well as all the finite difference expressions that are necessary for programming, can be found in Ref. 23.

Let the plane electromagnetic wave of TE polarization fall from a semi-infinite nonabsorbent space, +, on a periodic relief boundary, S (grating), with a finitely conductive in general semi-infinite space, −. The section of this surface by plane XY is described by function $f(x)$. The surface, S, is infinite in the direction of axes X and Z, d is a period, θ is an incident angle (with respect to axis OY), h is a groove depth, and $\mathbf{n}$ is a vector normal to the surface (directed from − to +). Inside the finitely conductive metal there is an electromagnetic field satisfying the boundary conditions on surface S and there is a current with a finite volume density. From the direction of the + medium ($y > 0$) the plane electromagnetic wave with the wave vector $\mathbf{k}^+$, in our case lying in the XY plane, is propagating. In this case a wave of any polarization can be represented as a sum of waves with TE (p) and TM (s) polarizations. There are only three field components (for the chosen polarization plane these are E_z, H_x, and H_y) that satisfy the homogeneous scalar Helmholtz–Kirchhoff equation for the medium with permittivity ϵ and vacuum magnetic permeability μ_0 (hereafter the case of nonmagnetic media is considered):

$$\Delta U + k^2 U = 0, \tag{2.1}$$

where U is any field component, $k = |\mathbf{k}| = \omega\sqrt{\epsilon}\sqrt{\mu_0}$, where ω is a cyclic frequency. The incident field $\mathbf{U}^i$ at

point M (x, y), which is above the grating surface, can be represented as

$$\mathbf{U}^i = \exp\{ik^+[\sin(\theta)x - \cos(\theta)y]\}\mathbf{e}_z, \qquad (2.2)$$

where $k^+ = k_0\sqrt{\epsilon^+} = 2\pi\sqrt{\epsilon^+}/\lambda_0$, where λ_0 is a wavelength in vacuum, and $\mathbf{e}_z$ is the direction of axis Z. The time factor $\exp(-i\omega t)$ hereafter is dropped.

For the basic types of polarization states, the diffraction of the incident wave results in formation of a diffracted field of the same polarization in the space above the grating. In the case of arbitrary polarization of the incident field the diffracted field polarization depends on the grating properties.[10] The total field in the space above the grating can be represented as the sum of the diffracted and the incident fields:

$$\mathbf{U} = \mathbf{U}^i + \mathbf{U}^d. \qquad (2.3)$$

It is possible to determine the diffracted field above the finitely conductive grating on the assumption that a field identical to this can arise as a result of the existence of some current flowing in the empty space on the surface, coinciding with the grating surface. In the case of TE polarization an electromagnetic field identical to the diffracted field can be induced by the electrical surface current. The density of this current $\mathbf{j}_e$ denoting a current j_e running through the unit of contour length on surface S in plane XY, perpendicular to this contour, can be represented as

$$\mathbf{j}_e = j_e\delta(x - x')\delta[y - f(x')]\mathbf{e}_z, \qquad (2.4)$$

where the product of the Dirac delta functions $\delta(x - x')\delta[y - f(x')]$ is equal to unity at $x = x'$ and $y = f(x')$ and to zero otherwise. It follows from Maxwell's equations for the field formed in the upper space by this electric current that the magnetic-field amplitude satisfies the nonuniform scalar-wave equation:

$$\Delta E + (k^+)^2E = -i\omega\mu_0 j_e\delta(x - x')\delta[y - f(x')]. \qquad (2.5)$$

The total field and, on the basis of Eq. (2.3), the diffracted field that satisfies Eq. (2.5), can be calculated as Helmholtz–Kirchhoff integrals on the closed infinite surface, S^+, taking into account the radiation condition:

$$E^d = \int_{S+} = \int_S \Gamma^+(x, y, s')\Phi(s')\mathrm{d}s', \qquad (2.6)$$

where s' is a curvilinear coordinate along the profile corresponding to the rectangular coordinates $[x', f(x')]$ and $\Phi(s') = -i\omega\mu_0 j_e\delta(x - x')\delta[y - f(x')]$. The elementary solution of the Helmholtz equation, function $\Gamma^+(x, y, s')$, is called the upper half-space Green's function.[10]

The integration over the entire surface, S, can be reduced to integration over one grating period, taking into account the quasi-periodicity property[23] (Floquet theorem) of the incident field [Eq. (2.2)] and the diffracted field [Eq. (2.6)]. Therefore the integral in Eq. (2.6) can be considered as a sum of integrals over an infinite number of grating periods. The upper half-space Green's function can be represented as an expansion in the plane wave series:

$$\Gamma^+(x, y, s') = \left\{\sum_{-\infty}^{\infty} \exp[i\alpha_n(x - x') + i\gamma_n{}^+|y - f(x')|]/\gamma_n{}^+\right\}\Big/(2id), \qquad (2.7)$$

where $K = 2\pi/d$, $\alpha_n = nK + \alpha_0$, $\alpha_0 = k^+\sin(\theta)$, and $\gamma_n{}^+ = [(k^+)^2 - \alpha_n{}^2]^{1/2}$, the y components of the wave vectors. The Green's function in Eq. (2.7) represents the radiation function of an infinite set of filiform sources a distance d from one another and whose radiation phase is taken into account by the exponential factor. The number of expansion terms in Eq. (2.7) can be optimized in the numerical realization. Thus the integral over one period is equivalent to the integral over the entire surface, S.

Considering the quasi-periodicity and taking into account that $\mathrm{d}s' = [1 + f(x')]\mathrm{d}x'$, the integrands in Eq. (2.6) can be replaced by new ones of the following kind:

$$\begin{aligned}\Psi[x', f(x')] &= \Phi[x', f(x')]\exp(-i\alpha_0 x') \\ &\quad \times \{1 + [f(x')]^2\}^{1/2}, \\ G^+(x, y, s') &= \exp(i\alpha_0 x)\left\{\sum_{-\infty}^{\infty} \exp[iKn(x - x') \right. \\ &\quad \left. + i\gamma_n{}^+|y - f(x')|]/\gamma_n{}^+\right\}\Big/(2id). \qquad (2.8)\end{aligned}$$

Now the integral of Eq. (2.6) can be represented as an integral taken over one grating period:

$$E^d = \int_d G^+[x, x', y, f(x')]\Psi[x', f(x')]\mathrm{d}x'. \qquad (2.9)$$

The integral in Eq. (2.9) in the case of TE polarization describes the tangential component of the electric field, which on the surface over which the electric current flows must be continuous. Therefore, at the crossing of the surface, S, by point M (x, y), the field described by the integral in Eq. (2.9) must be continuous. This indeed takes place, because the Green's function logarithmic singularity present in Eqs. (2.8) at $x = x'$ and $y = f(x')$ is integrable. The total field [Eq. (2.3)] in all the space is equal to the sum of the fields, one of which is defined by the integral in Eq. (2.9) and the other is the incident field [Eq. (2.2)]. Thus the limiting value of a tangential component of the complete field E^+ while an observation point M (x, y), situated above the grating, is moving to a point $[x, f(x)]$ on the surface, S, is equal to the total field value at this point:

$$E^+[x, f(x)] = E^i[x, f(x)] + \int_d G^+[x, x', f(x), f(x')]\Psi[x', f(x')]\mathrm{d}x'. \qquad (2.10)$$

The normal derivative of the electric field for the case of TE polarization is proportional to the magnetic-field tangential component, which in the presence of a surface electric current has a discontinuity equal to the current density:

$$H_t^+ - H_t^- = j_e, \tag{2.11}$$

where H_t^+ and H_t^- are the limiting values of the magnetic-field tangential components when an observation point is approaching the surface, S, from above and from under the surface, respectively. Hence the discontinuity of the electric-field normal derivative satisfies the condition

$$(\mathrm{d}E/\mathrm{d}n)^+ - (\mathrm{d}E/\mathrm{d}n)^- = -i\omega\mu_0 j_e. \tag{2.12}$$

The differentiation of the value [Eq. (2.10)] along the normal gives the half-sum of the limiting values of the field's normal derivative, which are obtained at the approach of an observation point M (x, y) to a point on the surface from below and above:

$$[(\mathrm{d}E/\mathrm{d}n)^+ + (\mathrm{d}E/\mathrm{d}n)^-]/2 = \mathrm{d}E^i[x, f(x)]/\mathrm{d}n + \int_d \{\mathrm{d}G^+[x, x', f(x), f(x')]/\mathrm{d}n\}\Psi[x', f(x')]\mathrm{d}x'. \tag{2.13}$$

From this, using Eqs. (2.8), (2.9), and (2.12), we obtained for the normal derivative limiting value, moving an observation point to the surface, S, from above,

$$\begin{aligned}\{\mathrm{d}E[x, f(x)]/\mathrm{d}n\}^+ = {} & \mathrm{d}E^i[x, f(x)]/\mathrm{d}n + 0.5\Psi \\ & \times [x', f(x')]\exp(i\alpha_0 x')/ \\ & \{1 + [f'(x')]^2\}^{1/2} + \int_d \{\mathrm{d}G^+ \\ & \times [x, x', f(x), f(x')]/\mathrm{d}n\} \\ & \times \Psi[x', f(x')]\mathrm{d}x'.\end{aligned} \tag{2.14}$$

Thus the complete field value and its normal derivative in the upper medium and on the boundary with the medium surface are expressed with one unknown scalar function Ψ. The diffracted field is calculated by Eq. (2.9). The Green's function normal derivative, present in Eqs. (2.13) and (2.14), is defined as

$$\begin{aligned}\mathrm{d}G^+[x, x', y, f(x')]/\mathrm{d}n = {} & \sum_{n=-\infty}^{\infty} \exp(i\alpha_0 x)/ \\ & \{2d[1 + f'(x)^2]^{1/2}\} \\ & \times \{\mathrm{sign}[f(x) - f(x')] \\ & - f'(x)\alpha_n/\gamma_n^+\}\exp[iKn(x \\ & - x') + i\gamma_n^+|f(x) \\ & - f(x')|],\end{aligned} \tag{2.15}$$

where the sign function $\mathrm{sign}[f(x) - f(x')]$ is equal to 1 if $[f(x) - f(x')] \geq 0$ and equal to -1 otherwise.

When the boundary conditions on the surface are used, it is possible to determine the values of the field and its normal derivative on the same surface in the lower medium. In the case of TE polarization the value of the field and its normal derivative on the interface inside the medium are equal to the corresponding values in the upper medium, Eqs. (2.10) and (2.14). If all the space is considered filled with substance, knowledge of the values of the field and its normal derivative in this substance on the surface, coincident with the initial medium interface surface, allows one to describe the field under the surface also by using the Helmholtz–Kirchhoff integral.[23] The Green's function and its normal derivative in this integral represent expressions similar to those used for the upper space in Eqs. (2.8) and (2.15). They are obtained by replacement of values γ_n^+ by the corresponding values γ_n^- for the substance under consideration:

$$\gamma_n^- = [(k^-)^2 - \alpha_n^2]^{1/2}, \qquad \mathrm{Im}(\gamma_n^-) > 0, \tag{2.16}$$

where $k^- = k_0\sqrt{\epsilon^-}$ and ϵ^- is the permittivity of the lower medium.

The integral equations for function Ψ are obtained on condition that in the considered integral an observation point is moving from the lower medium onto the surface of integration. Using Eqs. (2.10) and (2.14), as well as the considered boundary conditions, we finally obtained an integral equation for determining the unknown function Ψ:

$$\begin{aligned}E^i(x)/2 + \int_d & [G^-(x, x')\mathrm{d}E^i(x')/\mathrm{d}n' \\ & + E^i(x')\mathrm{d}G^-(x, x')/\mathrm{d}n']\mathrm{d}x' \\ = {} & -0.5\int_d G^-(x, x')\Psi(x')\mathrm{d}x' \\ & - 0.5\int_d G^+(x, x')\Psi(x')\mathrm{d}x' \\ & - \int\int_d [G^+(x', x'')\mathrm{d}G^-(x, x'')/\mathrm{d}n'' \\ & - G^-(x, x'')\mathrm{d}G^+(x', x'')/\mathrm{d}n'']\Psi(x')\mathrm{d}x'\mathrm{d}x'',\end{aligned} \tag{2.17}$$

where G^- is the Green's function for the lower medium and $\mathrm{d}G^-/\mathrm{d}n'$ and $\mathrm{d}G^-/\mathrm{d}n''$ are taken as positive.

In the upper medium the amplitudes for diffraction order number n can be obtained from Eq. (2.9) and the Rayleigh expansion [see Eq. (3.3)] for the plane waves by equating coefficients for the corresponding harmonics:

$$\begin{aligned}A_n^+ = -0.5i/(\mathrm{d}\gamma_n^+)\int_d \{\exp[-i\gamma_n^+ f(x') \\ - inKx']\Psi[x', f(x')]\}\mathrm{d}x'.\end{aligned} \tag{2.18}$$

In practice it is very important to know an absolute diffraction grating efficiency E_n^+. It is defined as energy flux going off the grating in the nth order per

incident energy flux unit. Then for the y component of the Umov–Poynting vector we obtain

$$E_n^+ = |A_n^+|^2 \gamma_n^+ / \gamma_i, \tag{2.19}$$

where $\gamma_i = \cos(\theta)$. When the Umov–Poynting theorem is used, it is also possible to determine the energy W_A absorbed by the grating material for a time unit. It is equal to the integral of an energy-flux density normal component $\mathbf{w}^-$, taken over the lower closed infinite surface, S:

$$W_A = \int_{S-} = \int_S \mathbf{w}^- \mathbf{n} \mathrm{d}s', \tag{2.20}$$

where $\mathbf{w}^- = \mathbf{E}^- \times \mathbf{H}^-$ is the Umov–Poynting vector in the lower medium. Taking into account Eq. (2.5), the quasi-periodicity property of the field, and the complex character of the amplitudes and their normal derivatives, it is easy to calculate the value W_A averaged over time:

$$E_A = 0.5 \int_d \mathrm{Re}[E^-(\mathrm{d}E/\mathrm{d}n)^{-*}/(i\omega\mu_0)]\mathrm{d}s', \tag{2.21}$$

where E^- is a field amplitude in the lower medium and $(\mathrm{d}E/\mathrm{d}n)^{-*}$ is a conjugate-complex value of the field amplitude normal derivative in the lower medium. The value E_A, normalized to the incident field energy flux unit, added to the sum of the efficiencies E_n^+ of all propagating harmonics represents the generalization of the energy conservation law for a finite-conductive grating. Knowledge of the accurate value of E_A for a grating represents one of the basic criteria for testing the correctness and reliability of the developed programs,[24] and it is especially important for investigations in the soft-x-ray–EUV range.

The solution of the integral equations is found by the known method of moments (the collocation method), based on replacement of the integral equation by a system of linear algebraic equations. It assumes finding N values of an unknown quasi-periodic function Ψ, which is approximated by a step function at N points in one period of the grating. At the realization of the calculation for gratings with a real groove profile, it is necessary for the correct account of the surface relief to use the number of collocation points, which is not less than the number of measured values of profile heights. As a rule the number of measured points on the surface is a hundred to several hundreds, and this does not limit the described integral approach and the programs developed on its basis. For profiles with very steep facets or large height differences, it is better to choose the points for integration equidistantly along the boundary surface as described in Ref. 23.

The developed method has a steady and fast convergence for the smallest values of the wavelength-to-period ratio (down to 10^{-6}) and for any other parameters. Optimizing the number of expansion terms for the Green's functions and their derivatives is not required as a rule, and an account of $N/2$ terms is optimal.[23] Also, an explicit allocation of the logarithmic singularity of the Green's functions is not necessary.

3. Modified Integral Method Applied to a Multilayer Grating

When considerations similar to those applied above for one medium boundary are used, it is possible to write down on the basis of the second Green's formula and boundary conditions a system of integral equations similar to Eqs. (2.10) and (2.14) for a multilayer grating consisting of KS_k boundaries, beginning from the first upper boundary:

$$\begin{aligned}
E_1(s_1)/2 = {} & E^i/2 + \int_{S1} G_1^+(s_1, s_1')[\mathrm{d}E_1(s_1')/\mathrm{d}n \\
& - \mathrm{d}E^i(s_1')/\mathrm{d}n]\mathrm{d}s_1' \\
& + \int_{S1} [\mathrm{d}G_1^+(s_1, s_1')/\mathrm{d}n'][E_1(s_1') \\
& - E^i(s_1')]\mathrm{d}s_1', \\
E_k(s_k)/2 = {} & \int_{Sk} G_k^-(s_k, s_k')[\mathrm{d}E_k(s_k')/\mathrm{d}n]\mathrm{d}s_k' \\
& - \int_{Sk} [\mathrm{d}G_k^-(s_k, s_k')/\mathrm{d}n']E_k(s_k')\mathrm{d}s_k' \\
& + \int_{Sk+1} G_{k+1}^+(s_k, s_{k+1}') \\
& \times [\mathrm{d}E_{k+1}(s_{k+1}')/\mathrm{d}n]\mathrm{d}s_{k+1}' \\
& + \int_{Sk+1} [\mathrm{d}G_{k+1}^+(s_k, s_{k+1}')/\mathrm{d}n'] \\
& \times E_{k+1}(s_{k+1}')\mathrm{d}s_{k+1}', \\
E_{k+1}(s_{k+1})/2 = {} & \int_{Sk+1} G_{k+1}^+(s_{k+1}, s_{k+1}') \\
& \times [\mathrm{d}E_{k+1}(s_k')/\mathrm{d}n]\mathrm{d}s_k' \\
& + \int_{Sk+1} [\mathrm{d}G_{k+1}^+(s_{k+1}, s_{k+1}')/\mathrm{d}n'] \\
& \times E_{k+1}(s_{k+1}')\mathrm{d}s_{k+1}' - \int_{Sk} G_k^-(s_{k+1}, s_k') \\
& \times [\mathrm{d}E_k(s_k')/\mathrm{d}n]\mathrm{d}s_k' \\
& - \int_{Sk} [\mathrm{d}G_k^-(s_{k+1}, s_k')/\mathrm{d}n']E_k(s_k')\mathrm{d}s_k', \\
E_K(s_K)/2 = {} & -\int_{SK} G_K^-(s_K, s_K')[\mathrm{d}E_K(s_K')/\mathrm{d}n]\mathrm{d}s_K' \\
& - \int_{SK} [\mathrm{d}G_K^-(s_K, s_K')/\mathrm{d}n']E_K^-(s_K')\mathrm{d}s_K', \\
& k = 1, K-1,
\end{aligned} \tag{3.1}$$

where E_k is a z component of the electric field for the kth profile and the Green's function $G_k^{\pm}$ and its normal derivative are defined by Eqs. (2.8) and (2.15), taking into account the propagation constants $\gamma_{k,n}^{\pm}$ for regions lying above the + or lower − kth boundary. The normal derivative of the incident field is calculated as

$$dE^i(s_1')/dn = -i\{\gamma_i + \alpha_0 df_1[x'(s_1')]/ds_1'\} \times \exp\{-i\gamma_i f_1[x'(s_1')]\}, \quad (3.2)$$

where $f_1[x'(s_1')]$ is the first profile function, and the coordinate $x'(s_1')$ is defined by a curvilinear coordinate s_1', taken on this profile. Equations (3.1) contains $2K$ equations and $2K$ unknown electric fields and their normal derivatives. For $K = 2$ it is possible to obtain from Eqs. (3.1) the system of integral equations in the operator representation.[31,32]

In the upper medium the amplitudes for the diffraction order number n can be obtained from Eqs. (2.8), (2.14) and the first equation in Eq. (3.1) by equating the coefficients for the corresponding harmonics to the coefficients of the Rayleigh expansion for plane waves:

$$E_1(x, y) = \sum_{n=-\infty}^{\infty} A_n[\exp(inKx + i\gamma_{1,n}{}^{+}y)]. \quad (3.3)$$

The amplitudes for the reflected orders are determined in this case by using

$$A_n = (0.5/d)\int_{S1} [((-i\gamma_{1,n}{}^{+})[dE_1(s_1)/dn - dE^i(s_1)/dn] + \{dx(s_1)/ds_1 - [df_1(s_1)/ds_1]\alpha_n/\gamma_{1,n}{}^{+}\}[E_1(s_1) - E^i(s_1)])\exp[-i\gamma_{1,n}{}^{+}f_1(s_1) - inKx(s_1)]]ds_1. \quad (3.4)$$

Efficiencies for the propagating orders are calculated as usual from Eq. (2.19).

A joint solution of $2K$ pair equations from Eqs. (3.1) for the soft-x-ray–EUV range is a difficult but feasible task[32] for a modern personal computer. This is due to the fast attenuation of the fields and the very strong convergence of the created modified integral method in the short-wavelength range.[14] At the numerical realization we used subroutines created for calculations of the uncoated gratings from Section 2. For the case of a large number of layers, additional simplifications resulting in considerable reduction in the requirements for RAM and calculating time can be made at the stage of optimization of the code, for example, with an internal program memory cache for repetitive calculations. The developed program using the results in Sections 2 and 3 has been tested by all known methods: by investigating convergence with respect to the cutting-off parameter and to the number of expansion terms of the Green's functions and their derivatives,[23] by calculating the energy balance for finite-conducting gratings,[23,29] by the reciprocity theorem,[10] by comparisons with the reflectance of multilayer mirrors,[17,33] and by reproducing many published numerical[10,12,13,17,18,23,30] and experimental results[1–3,5–7,24–29,34] that are discussed further.

4. Grating Parameters and Efficiency Measurements

The investigated master[5] grating was fabricated by Spectrogon UK Ltd. (formerly Tayside Optical Technology). The groove pattern was fabricated in fused silica by using a holographic technique. The groove pattern was ion-beam etched to produce an approximately triangular, blazed groove profile. The grating has 2400 grooves/mm, a concave radius of curvature of 2.0 m, and a patterned area of 45 mm × 35 mm size. The master grating was uncoated.

The replica[6] of the master grating was produced by Hyperfine Inc. As a result of the replication process the replica grating had an oxidized aluminum surface. A thin SiO_2 coating was applied to the oxidized aluminum surface to reduce microroughness.

The surfaces of the master grating and the replica grating were characterized by a Topometrix Explorer Scanning Probe Microscope, a type of AFM. The AFM images typically had 500 × 500 pixels and a scan range of 1–20 μm (pixel size, 2–40 nm). The silicon probe had a pyramid shape. The base of the pyramid was 3–6 μm in size, the height of the pyramid was 10–20 μm, and the height-to-base ratio was ~3. The tip of the pyramid had a radius of curvature of less than 20 nm. The AFM scans were performed with the noncontact resonating mode, where the change in the oscillation amplitude of the probe is sensed by the instrument.

A surface topology reference sample was used to optimize the AFM scanning parameters, to calibrate the height scaling of the instrument, and to evaluate the performance of the AFM. This was essential for an accurate characterization of the gratings. The surface topology reference sample consisted of an array of approximately square holes fabricated on the silicon dioxide surface of a silicon die by VLSI Standards Inc. The top surface of the die was coated with a thin layer of platinum. The hole array had a pitch of 3 μm and a hole depth of 18 nm.

A typical groove profile derived from the AFM image with 210 points of the master grating is shown in Fig. 1 (by curve 1). The groove profile is approximately triangular in shape with rounded corners and troughs and with facet angles of 2.5° and 5.5°. The average groove height derived from the AFM images is 7.5 nm. A typical groove profile derived from the AFM scans (1 μm in size) of the replica grating is shown in Fig. 1 by curve 2. An approximately triangular groove profile has facet angles of 3.4° and 6.2°. The average groove depth derived from the AFM images is 9.0 nm. These values of the facet angles and the groove depth are larger than the corresponding values for the master grating. Thus the grooves of the replica grating are deeper and the facet angles are steeper compared with those of the master grating.

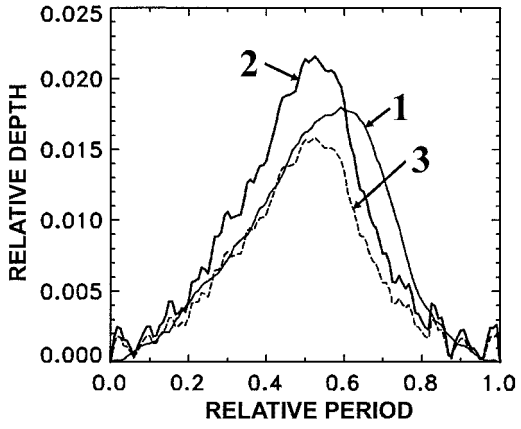

Fig. 1. Groove profiles derived from the AFM images of the 2400-groove/mm gratings: curve 1, 7.5-nm depth master AFM profile; curve 2, 9.0-nm depth replica AFM profile; curve 3, 6.6-nm depth scaled replica AFM profile. The depth is relative to the period.

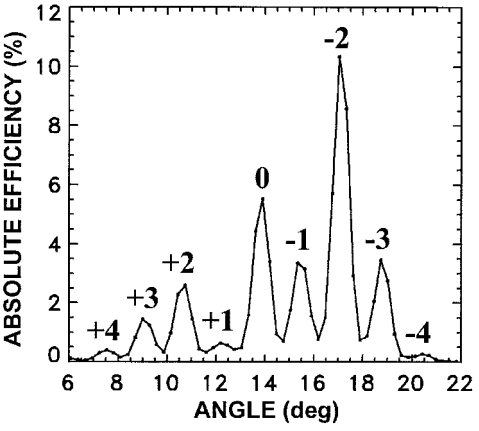

Fig. 2. Measured efficiencies of the multilayer grating at a wavelength of 11.37 nm. The angle of incidence is 13.9°.

The microroughness was determined by integrating the power spectral density function over the $4-40\text{-}\mu m^{-1}$ spatial-frequency range for the AFM data of the master grating. The rms microroughness σ of the master grating was 0.32 nm. By comparison the microroughness of the replica grating measured by the same type of AFM instrument in the $4-40\text{-}\mu m^{-1}$ frequency range was 0.7 nm, and this implies that the replica grating is significantly rougher than the master grating. This roughness may result from the replication process, which for a concave grating is at least a two-step process. Furthermore the master grating was fabricated on a fused silica surface by a holographic technique and was ion-beam polished, while the oxidized aluminum surface of the replica grating may contribute to its larger microroughness.

Multilayer[7] gratings were produced by application of Mo_4Ru_6–Be multilayer coatings to two replicas of the holographic master grating. Beryllium-based multilayer coatings can provide substantial reflectance at wavelengths near 11 nm. A newly developed multilayer coating, Mo_4Ru_6–Be, has several beneficial properties.[35] The absorber layer consists of an alloy material with a composition of Mo_4Ru_6. A normal-incidence reflectance of 69.3% at a wavelength of 11.4 nm was achieved.[35] The multilayer's stress, which is composition dependent, varies between −30 and +30 MPA and can be designed to be nearly zero. Owing to the microstructural properties of the layers (the alloy layers are amorphous and the Be layers are polycrystalline), the coating smoothes the high-frequency roughness of the substrate. Since the efficiency of the multilayer-coated grating in the short-wavelength region strongly depends on roughness, a multilayer coating that can smooth the grating surface is beneficial.

Such a Mo_4Ru_6–Be multilayer coating with 50 bilayers was applied to the grating substrate. The coating was deposited by the magnetron-sputtering technique. As determined below the total thickness of the coating on the grating was 301.5 nm. This coating thickness was much larger than the calculated grating average groove depth of 6.6 nm.

The efficiencies of the master, uncoated replica, and multilayer replica gratings were measured with the Naval Research Laboratory beamline X24C at the National Synchrotron Light Source at the Brookhaven National Laboratory. The synchrotron radiation was dispersed by a monochromator that had a resolving power of 600. Thin filters suppressed the radiation from the monochromator in the higher harmonics. The wavelength scale was established by the geometry of the monochromator and the absorption edges of the filters. The gratings were oriented so that the groove facets with the larger facet angle (measured from the surface of the grating substrate) faced the incident beam. The incident radiation was ~80% polarized with the electric-field vector in the plane of incidence. In this orientation the electric-field vector was almost perpendicular to the grating grooves. The 13.9° angle of incidence, used when measuring the multilayer grating, permitted observation of a wide angular range without obscuration of the higher diffraction orders by the detector.[7] At fixed incident wavelengths the detector was scanned in angle about the grating. The incident beam was ~1 mm in size. Measurements were performed at a number of fixed wavelengths in the 10.5–13.0-nm range and in the 25–50-nm wavelength range. From the efficiency measurements performed at a number of fixed incident wavelengths, it was found that the peak −2 efficiency of the multilayer grating occurred at a wavelength of 11.4 nm. Low efficiencies[7] could be measured because of the relatively high multilayer reflectance and groove efficiency of the grating and the high sensitivity and low background current (3 pA) of the silicon photodiode detector (type AXUV-100G provided by International Radiation Detectors, Inc.).

As an example the efficiencies of the multilayer grating measured in different orders at an incident wavelength of 11.37 nm are shown in Fig. 2. The 0.5° widths (at the half-peak efficiency levels) of the

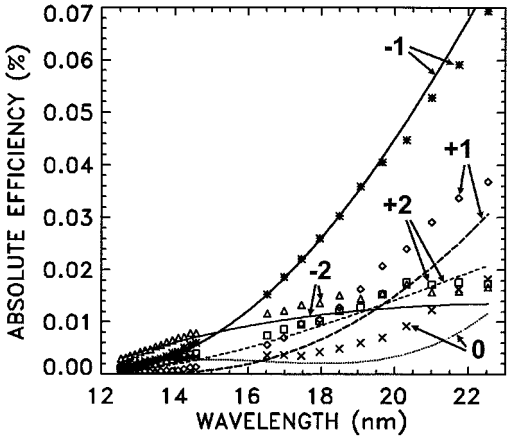

Fig. 3. Comparison of the measured (data points) and calculated (curves) master grating efficiencies for the indicated diffraction orders in the 12.5–22.5-nm wavelength range.

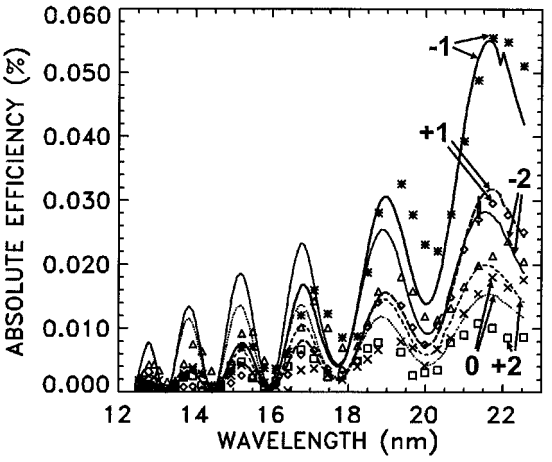

Fig. 4. Comparison of the measured (data points) and calculated (curves) replica grating efficiencies for the indicated diffraction orders in the 12.5–22.5-nm wavelength range.

orders shown in Fig. 2 result from the 1-mm slit over the detector.

5. Choice of an Efficiency Calculation Model and Comparison of the Calculations with the Measurements

The modeling of three various types of gratings has been carried out by only one computer program, PCGrate,[24] based on the modified integral method described above. For the calculations the groove profiles obtained in Section 4 from the averaged AFM measurements have been used. Because the calculations were performed in a wide range of wavelengths from 4.5 to 50 nm, choosing the correct refractive indices of the layer and substrate materials was important. The refractive-index data derived from Henke *et al.*,[36] which are usually used for calculations in the soft-x-ray–EUV range, were usable only to as long as a wavelength of 43 nm. Near this wavelength the real part of the refraction indices of the materials becomes stepwise equal to unity. Therefore, for calculations with wavelengths longer than 43 nm, we have used the experimental values of refractive indices from Refs. 37 and 38.

For rigorous modeling of the master grating efficiency, no additional assumptions on the calculation model were required. We used an averaged groove profile obtained from the AFM data with subsequent processing[5] (Fig. 1) and refractive indices in the 12.5–22.5-nm range from Ref. 36. The calculations were performed with 210 collocation points, without optimization of the numbers of expansion terms of the Green's functions and their normal derivatives. The error of all calculations with respect to the total energy balance was approximately 10^{-4} of absolute percents. Owing to the small amplitude of the random microroughnesses and the not very short wavelength range, the influence of microroughnesses on the efficiencies for this grating was not taken into account. The calculated curves and the data points of the measured efficiencies in the 0, ± 1, and ± 2 orders are given for comparison in Fig. 3. For the -1 order the difference between the measured and the calculated values is less than 10 relative percents for all reliable points. All compared values are in very good numerical agreement, especially if one takes into account the very small absolute efficiency values and the strong influence of the form and the depth of a grating profile on the efficiency in this range. The calculating time on a Dual Intel Pentium III 1-GHz, 256-Kbyte Cache Workstation with 512 Mbyte of RAM and a 133-MHz Bus Clock working under MS Windows 2000 Pro is $\sim$13 s/point.

For development of the computational model of the replica grating in the same wavelength range, in addition to information on the exact groove profile obtained from the average AFM measurements (Fig. 1) and the refractive indices taken from Ref. 36, we have used some additional assumptions on the coating materials of the grating and their thicknesses. As mentioned above the replica grating had an aluminum surface with a thin layer of oxide. In addition the grating surface was coated with a thin film of SiO_2 for reduction of the microroughness. As a result the efficiency of this grating measured as a function of wavelength had an oscillating behavior. To determine the thickness of the Al_2O_3 and SiO_2 layers, a procedure based on analysis of local coincidences of the calculated and the measured maxima for various wavelengths in the 0 diffraction order was used.[6] The thickness of Al_2O_3 equal to 3 nm and that of SiO_2 equal to 74.3 nm were determined with an uncertainty of 0.5 nm in both cases. Although the replica grating microroughness was 2 times higher than that of the master grating, we have neglected its effect on the efficiency values calculated for the 12.5–22.5-nm range. The calculated curves and the points corresponding to the measured efficiency for the 0, ± 1, and ± 2 orders are given for comparison in Fig. 4. The general agreement in the maximum and the minimum positions as well as in the efficiency values is good. For the -1 order the rms difference in the data for the model and the experiment is equal to 0.0039%, which is approximately a quarter of the

mean efficiency value for this order in the investigated range. An account of the random microroughness component in the calculations for the short-wavelength part of the range would make the efficiency values more accurate and reduce the rms difference between the model and the experiment data. The time required for calculation of one point of the replica grating was manageable and approached the calculation time for the uncoated master grating, while fast caching for repeating values and acceleration of the code was used.

The grating most difficult for modeling was the multilayer grating as one might expect. In this case the average depth of modulation of the layers was scaled to achieve the best agreement with the experimental data near 11.4 nm where the efficiency was maximal. The depth of the profile of the (replica) grating substrate was 9.0 nm, as derived from the AFM measurements in Section 4. During the process of coating the grating substrate with multiple layers to produce a multilayer grating, a smoothing of the groove profile takes place. As a result the depth of modulation of the upper layers decreases appreciably. Because the influence of diffraction by the upper layers on an absolute grating efficiency is higher than that by the lower layers, and because there was no information on a change in the profile modulation depth (and the profile deformation) from one layer to another, a model with average (with respect to all layers) profile modulation depth was used. By scaling the initial groove profile of the replica grating, a groove profile was determined that resulted in the smallest least-squares difference between the calculated and measured efficiencies at a wavelength of 11.4 nm. The resulting depth was 6.6 nm, which means that the profile becomes appreciably smoother in the upper layers. A scaled averaged groove profile used in the efficiency calculations of the multilayer grating is shown in Fig. 1 by curve 3.

Another problem in development of the efficiency calculation model for the multilayer grating was the choice of the refractive indices of the layer materials and their thicknesses. Efficiency measurements for the multilayer grating were made in two widely separated wavelength regions. For wavelengths as long as 40 nm, optical constants derived from Ref. 36 were used. For wavelengths longer than 40 nm the experimental values from Refs. 37 and 38 were used. From the maximum reflectance of a multilayer Mo_4Ru_6–Be coating with 50 layers, a bilayer thickness of 6.03 nm and the ratio of the beryllium layer thickness to the bilayer thickness equal to 0.58 were determined.[7] It was also determined that the calculated efficiency in the long-wavelength range depended significantly on the degree of the upper-beryllium-layer oxidation. For example, the efficiency in 0 and ± 1 orders for the unoxidized upper beryllium layer and the completely oxidized upper beryllium layer differ by a factor of ~ 3 for a wavelength of 40 nm. Since the effect of the beryllium oxide (BeO) film thickness for short wavelengths is insignificant, we determined the oxide film thickness by the best agreement of the efficiency values measured in the 25–40-nm range with those calculated with the least-squares method. The calculated value of the BeO film thickness thus obtained is equal with a small uncertainty to one-third of the Be layer thickness. The model with the upper one-third oxidized beryllium layer has been used in all calculations. Because of the lack of refractive indices data for BeO in the 40.5–50-nm range, for example, in Refs. 37 and 38, the uppermost Be layer was assumed to be unoxidized in this wavelength range. Note that a model with a completely oxidized upper layer and another type of groove profile were used in calculations in Ref. 7.

In the efficiency calculation model for the multilayer grating we have also taken into account the effect of the random roughness component of the layers, which affects appreciably the reflectivity in the short-wavelength range of the performed investigation. Considering the rms microroughness to be the same for all layers and equal to $\sigma = 0.7$ nm, we multiplied the obtained field amplitudes on the boundaries by the Debye–Waller factor that is equal to $\exp\{-[2\pi\sigma \cos(\varphi)/\lambda]^2\}$ in all investigated wavelength ranges. Such an approach is not rigorous for an accounting of the grating microroughness. The rigorous approach is based on the integration over an infinite number of grating periods for any (not necessarily Gaussian) roughness distribution function along the groove profiles, which excludes the opportunity to use the quasi-periodicity functions as done, for example, in Eqs. (2.8). However, comparisons of these two calculation methods, carried out by us in the investigation of the efficiency of uncoated gratings in the soft-x-ray–EUV range, have shown their practical identity, at least for the normal law of roughness distribution and for not too large values of their amplitudes and radii of correlation. This conclusion is also correct for multilayer gratings. Using the Debye–Waller factor reduces the calculation time by orders of magnitude, and presently it is the only feasible approach for multilayer gratings.

On the basis of the developed model of the multilayer grating the calculations of its absolute efficiency in the short-wavelength range, 11.1–12 nm [Fig. 5(b)], and in the long-wavelength range, 25–50 nm (Fig. 6), have been made. The curves in Fig. 5(a) and the points in Fig. 6 denote corresponding measured values. Comparing Fig. 5(a) with Fig. 5(b) allows one to consider the good agreement not only of the form and the efficiency curve position for the 0, ± 1, ± 2, ± 3, ± 4, and ± 5 orders but also of their absolute values. For example, the measured maximum efficiency value for the -2 order at 10.4 nm was 10.4%, and the corresponding calculated value was 11.5%. Thus the difference between the theory and the experiment, for this example, is ~ 10 relative percent, which is small considering the complexity of the model. Still smaller, on average, differences in the calculated and the measured efficiency values are observed in the long-wavelength range, which one can see in Fig. 6 for the presented curves for the 0 and

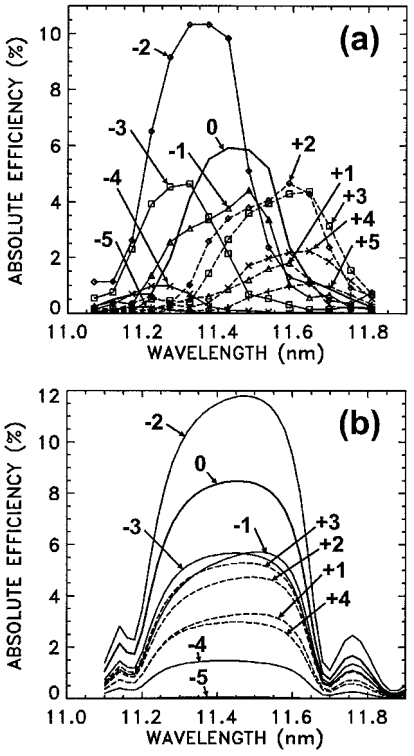

Fig. 5. Peak efficiencies (a) measured and (b) calculated at an angle of incidence of 13.9° for the multilayer grating for the indicated diffraction orders in the 11.1–12.0-nm wavelength range.

±1 orders. Somewhat larger theoretical efficiency values in Fig. 5(b) compared with the measured values in Fig. 5(a) can have several explanations. Foremost are the uncertainties in the refractive-index values and the profile deformation while coating layers are deposited. The calculation time of one point when one uses the above-mentioned computer varies from several tens of seconds to as many as several tens of minutes for the uncertainty lying in a range of 10^{-3} to 10^{-4} absolute percents.

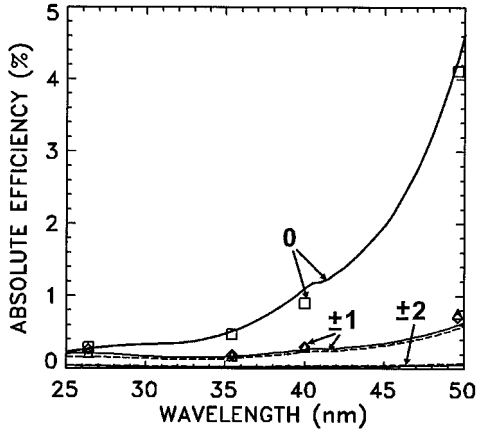

Fig. 6. Comparison of the measured (data points) and calculated (curves) multilayer grating efficiencies for the indicated diffraction orders in the wavelength range from 25 to 50 nm.

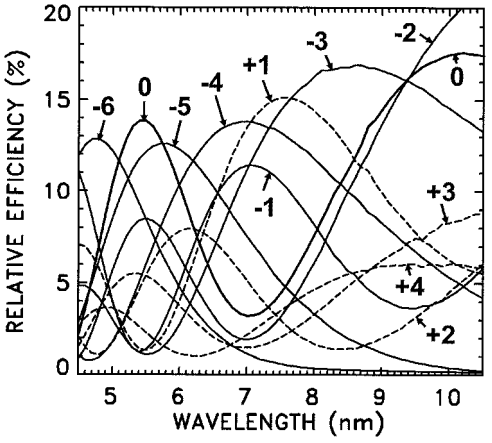

Fig. 7. Calculated relative efficiencies of the multilayer grating for the indicated diffraction orders in the 4.5–10.5-nm wavelength range.

6. Multilayer Grating Relative Efficiency in the 4.5–10.5-nm Range

The relative diffraction efficiency has also been calculated for the model of a multilayer grating, developed in Section 5, in the wavelength range of 4.5–10.5 nm. The relative efficiency is usually defined as the ratio of the absolute efficiency to the mirror reflectivity of a grating coating. In the shortest investigated wavelength range an absolute grating efficiency for near to normal incidence is approximately equal to the product of its ideal efficiency obtained in an assumption of perfect conductivity of the coating material by a reflectivity of the multilayer mirror coating the grating.[17] Our investigation, which has been carried out with refractive indices taken from Henke *et al.*,[36] basically confirms this rule for a multilayer grating with the real groove profile as well. Therefore it was interesting and useful to derive the wavelength dependence for the relative efficiency of the investigated multilayer grating in the short-wavelength range down to 4.5 nm. When multilayer coatings based on such pairs as Cr–C, Be–B_4C, Be–C, Be–Y, and Mo–Y are used, it is possible to obtain in some cases the theoretical maximum reflection for this range to as great as 40–50%. Taking into account a microroughness, $\sigma = 0.7$ nm, reflectance in practice will be approximately two times smaller. As shown in Fig. 7 the universal curves for the relative efficiency of a substrate grating with a groove depth of 6.6 nm have maxima in the 13–20% range for the negative orders. Thus the absolute efficiency of a grating with the appropriate coating in this range can reach 2.5–5%. These rather high values are also of particular interest because the greatest efficiency for the shortest wavelengths in the 4.5–7-nm range are reached in the high diffraction orders from −4 to −6. This means that a rather high efficiency at a high spectral resolution can be obtained for real gratings.[7]

7. Conclusion

The efficiency calculations in the 10.5–50-nm range are in good agreement with the measured efficiencies not only qualitatively, but also quantitatively, when one theoretical model for three similar gratings but of various types is used: the master grating, the replica grating, and the multilayer grating. For example, the most time-consuming modeling of the multilayer grating efficiency in −2 order near 11.4 nm gives a peak value of 11.5% compared with a measured value of 10.4%. The earlier calculated value for this peak was equal to 14%.[7] At longer wavelengths the relative differences between the measured and the calculated efficiencies are smaller.

It was not possible earlier to achieve such good agreement for gratings of this spectral range with real (measured with the help of the AFM) groove profiles because of the lack of a suitable theory and the difficulty in correctly choosing the calculation model. The developed modified integral method and the suitable computer programs, written on its basis, allow one to carry out rather easily a detailed systematic modeling on a standard personal computer. The rigorous calculation accounts for the real profile of the layers and their thickness as well as suitable refractive indices.

The analysis of the calculated curves for the multilayer grating relative efficiency in the 4.5–10.5-nm range indicates an opportunity to achieve rather high absolute efficiency values of 2.5–5% for the high diffraction orders, from −4 to −6 in the short-wavelength part of this range, by application of suitable multilayer coatings (Cr–C, Be–B_4C, Be–C, Be–Y, or Mo–Y) at low levels of microroughness (0.7 nm). This result provides good potential for designing instruments with high spectral resolution in the soft-x-ray–EUV range for the study of solar, astrophysical, and laboratory plasmas.

Although in the present work blazed gratings with approximately triangular groove profiles have been considered, a related computer model[24] has been applied to the analysis of multilayer laminar gratings with rectangular groove profiles. Good agreement was obtained between the measured and the calculated efficiencies of the multilayer laminar gratings. The computer model has been used for optimization of the multilayer laminar grating that will be utilized in the Extreme Ultraviolet Imaging Spectrometer on the Solar B spacecraft.[26]

This research was supported in part by NASA project W-19513.

References

1. J. F. Seely, R. G. Cruddace, M. P. Kowalski, W. R. Hunter, T. W. Barbee, J. C. Rife, R. Ely, and K. G. Stilt, "Polarization and efficiency of a concave multilayer grating in the 135–250-Å region and in normal-incidence and Seya–Namioka mounts," Appl. Opt. **34,** 7347–7354 (1995).
2. J. F. Seely, M. P. Kowalski, R. G. Cruddace, K. F. Heidemann, U. Heinzmann, U. Kleineberg, K. Osterried, D. Menke, J. C. Rife, and W. R. Hunter, "Multilayer-coated laminar grating with 16% normal-incidence efficiency in the 150-Å region," Appl. Opt. **36,** 8206–8213 (1997).
3. C. Montcalm, S. Bajt, and J. F. Seely, "MoRu–Be multilayer-coated grating with 10.4% normal-incidence efficiency near the 11.4-nm wavelength," Opt. Lett. **26,** 125–127 (2001).
4. V. V. Martynov, H. A. Padmore, Yu. Agafonov, and A. Yuakshin, "X-ray multilayer gratings with very high diffraction efficiency," in *Gratings and Grating Monochromators for Synchrotron Radiation*, W. R. McKinney and C. A. Palmer, eds., Proc. SPIE **3150,** 2–8 (1997).
5. M. P. Kowalski, J. F. Seely, L. I. Goray, W. R. Hunter, and J. C. Rife, "Comparison of the calculated and the measured efficiencies of a normal-incidence grating in the 125–225-Å wavelength range," Appl. Opt. **36,** 8939–8943 (1997).
6. J. F. Seely, L. I. Goray, W. R. Hunter, and J. C. Rife, "Thin-film interference effects of a normal-incidence grating in the 100–350-Å wavelength region," Appl. Opt. **38,** 1251–1258 (1999).
7. J. F. Seely, C. Montcalm, and S. Bajt, "High-efficiency MoRu–Be multilayer-coated gratings operating near normal incidence in the 11.1–12.0-nm wavelength range," Appl. Opt. **40,** 5565–5574 (2001).
8. A. I. Erko, B. Vidal, P. Vincent, Yu. A. Agafonov, V. V. Martynov, D. V. Roschupkin, and M. Brunel, "Multilayer grating efficiency: numerical and physical experiments," Nucl. Instrum. Methods A **333,** 599–606 (1993).
9. V. Martynov, B. Vidal, P. Vincent, M. Brunel, D. V. Roschupkin, Yu. Agafonov, A. Erko, and A. Yuakshin, "Comparison of modal and diffirential methods for multilayer gratings," Nucl. Instrum. Methods A **339,** 617–625 (1994).
10. R. Petit, ed., *Electromagnetic Theory of Gratings* (Springer-Verlag, Berlin, 1980).
11. L. I. Goray, "Nonscalar properties of high groove frequency gratings for soft-x-ray and XUV regions: the integral equation method," in *X-Ray and UV Detectors*, R. B. Hoover and M. W. Tate, eds., Proc. SPIE **2278,** 173–177 (1994).
12. M. Nevière and J. Flamand, "Electromagnetic theory as it applies to x-ray and XUV gratings," Nucl. Instrum. Methods **172,** 273–279 (1980).
13. H. A. Podmore, V. Martynov, and K. Holis, "The use of diffraction efficiency theory in the design of soft-x-ray monochromators," Nucl. Instrum. Methods A **347,** 206–215 (1994).
14. L. I. Goray, "Numerical analysis for relief gratings working in the soft-x-ray and XUV region by the integral equation method," in *X-Ray and UV Detectors*, R. B. Hoover and M. W. Tate, eds., Proc. SPIE **2278,** 168–172 (1994).
15. L. I. Goray, "Rigorous integral method in application to computing diffraction on relief gratings working in wavelength range from microwaves to x ray," in *Application and Theory of Periodic Structures*, T. Jannson and N. C. Gallagher, eds., Proc. SPIE **2532,** 427–433 (1995).
16. L. I. Goray and B. C. Chernov, "Comparison of rigorous methods for x-ray and XUV grating diffraction analysis," in *X-Ray and Extreme Ultraviolet Optics*, R. B. Hoover and A. B. Walker, eds., Proc. SPIE **2515,** 240–245 (1995).
17. B. Vidal, P. Vincent, P. Dhez, and M. Nevière, "Thin films and gratings: theories used to optimize the high reflectivity of mirrors and gratings for x-ray optics," in *Applications of Thin-Film Multilayered Structures to Figured X-Ray Optics*, G. F. Marshall, ed., Proc. SPIE **563,** 142–149 (1985).
18. M. Nevière, "Multilayer coated gratings for x-ray diffraction: differential theory," J. Opt. Soc. Am. A **8,** 1468–1473 (1991).
19. A. Sammar, J.-M. André, and B. Pardo, "Diffraction and scattering by lamellar amplitude multilayer gratings in the XUV region," Opt. Commun. **86,** 245–254 (1991).
20. V. I. Erofeev and N. V. Kovalenko, "Method of eigenvectors for numerical studies of multilayer gratings," X-Ray Sci. Technol. **7,** 75 (1997).

21. M. Nevière, "Bragg–Fresnel multilayer gratings electromagnetic theory," J. Opt. Soc. Am. A **11,** 1835–1845 (1994).
22. A. Sammar and J.-M. André, "Diffraction of multilayer gratings and zone plates in the x-ray region using the Born approximation," J. Opt. Soc. Am. A **10,** 600–613 (1993).
23. L. I. Goray, "Modified integral method for weak convergence problems of light scattering on relief grating," in *Diffractive and Holographic Technologies for Integrated Photonic Systems*, R. I. Sutherland, D. W. Prather, and I. Cindrich, eds., Proc. SPIE **4291,** 1–12 (2001).
24. Internet site, http://www.pcgrate.com.
25. J. F. Seely and L. I. Goray, "Normal incidence multilayer gratings for the extreme ultraviolet region: experimental measurements and computational modeling," in *X-Ray Optics, Instruments, and Missions II*, R. B. Hoover and A. B. Walker, eds., Proc. SPIE **3766,** 364–370 (1999).
26. J. F. Seely, "Multilayer grating for the extreme ultraviolet spectrometer (EIS)," in *X-Ray Optics, Instruments, and Missions IV*, R. B. Hoover and A. B. C. Walker, eds., Proc. SPIE **4138,** 174–181 (2000).
27. D. A. Content, "Diffraction grating groove analysis used to predict efficiency and scatter performance," in *Conference on Gradient Index, Miniature, and Diffractive Optical Systems*, A. D. Kathman, ed., Proc. SPIE **3778,** 19–30 (1999).
28. D. A. Content, "Grating groove metrology and efficiency predictions from the soft-x-ray to the far infrared," in *Optical Spectroscopic Techniques and Instrumentation for Atmospheric and Space Research IV*, A. M. Larar and M. G. Mlynczak, eds., Proc. SPIE **4485** (to be published).
29. L. I. Goray, "Modified integral method and real electromagnetic properties of echelles," in *Diffractive and Holographic Technologies for Integrated Photonic Systems*, R. I. Sutherland, D. W. Prather, and I. Cindrich, eds., Proc. SPIE **4291,** 13–24 (2001).
30. M. Nevière and F. Montiel, "Soft-x-ray multilayer coated echelle gratings: electromagnetic and phenomenological study," J. Opt. Soc. Am. A **13,** 811–818 (1996).
31. A. Pomp, "The integral method for coated gratings: computational cost," J. Mod. Opt. **38,** 109–120 (1991).
32. S. Yu. Sadov and L. I. Goray are preparing a manuscript to be called "The modified integral method for gratings covered with thin or thick layers of arbitrary shape."
33. A. Spiller and A. E. Rosenbluth, "Determination of thickness errors and boundary roughness from the measured performance of a multilayer coating," in *Applications of Thin-Film Multilayered Structures to Figured X-Ray Optics*, G. F. Marshall, ed., Proc. SPIE **563,** 221–236 (1985).
34. W. Jark, "Enhancement of diffraction grating efficiencies in soft-x-ray region by multilayer coating," Opt. Commun. **60,** 201–205 (1986).
35. S. Bajt, "Molybdenum-ruthenium/beryllium multilayer coatings," J. Vac. Sci. Technol. A **18,** 557–559 (2000).
36. A. L. Henke, E. M. Gullikson, and J. C. Davis, "X-ray interactions: photoabsorption, scattering, transmission, and reflection at E = 50–30,000 eV, Z = 1–92," At. Data Nucl. Data Tables **54,** 181–342 (1993). Updated optical constants were obtained from the Internet site, http://cindy.lbl.gov/optical_constants.
37. A. T. Arakawa, T. A. Callcott, and Y. C. Chang, "Beryllium (Be)," in *Handbook of Optical Constants of Solids II*, E. D. Palik, ed. (Academic, New York, 1991), pp. 421–433.
38. A. W. Lynch and W. R. Hunter, "Molybdenum (Mo)," in *Handbook of Optical Constants of Solids*, E. D. Palik, ed. (Academic, New York, 1985), pp. 303–313.